

The influence of air mass histories on radical species during POLARIS

J. M. Pierson

Universities Space Research Association

Seabrook, MD 20706

S.R. Kawa

NASA Goddard Space Flight Center, Greenbelt, MD 20771

R. J. Salawitch

NASA Jet Propulsion Laboratory, Pasadena, CA 91109

T. F. Hanisco, E. J. Lanzendorf and K. K. Perkins

Department of Chemistry and Department of Earth and Planetary Sciences

Harvard University, Cambridge, MA 02138

R. S. Gao

NOAA Aeronomy Lab, Boulder, CO 80303

R. C. Cohen

Department of Chemistry, University of California-Berkeley, Berkeley, CA 94720

Short title: INFLUENCE OF AIRMASS HISTORIES

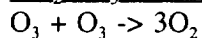
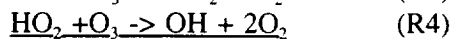
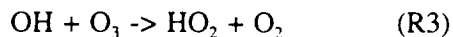
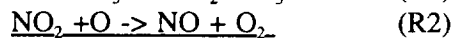
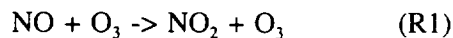
Abstract. The Goddard trajectory chemistry model was used with ER-2 aircraft data to test our current knowledge of radical photochemistry during the POLARIS (Polar Ozone Loss in the Arctic Region In Summer) campaign. The results of the trajectory chemistry model with and without trajectories are used to identify cases where steady state does not accurately describe the measurements. Over the entire mission, using trajectory chemistry reduces the variability in the modeled NO_x comparisons to data by 25% with respect to the same model simulating steady state. Although the variability is reduced, NO_x/NO_y trajectory model results were found to be systematically low relative to the observations by 20-30% as seen in previous studies. Using new rate constants for reactions important in NO_y partitioning improves the agreement of NO_x/NO_y with the observations but a 5-10% bias still exists. OH and HO_2 individually are underpredicted by 15% of the standard steady state model and worsen with the new rate constants. Trajectory chemistry model results of OH/ HO_2 were systematically low by 10-20% but improve using the new rates constants because of the explicit dependence on NO. This suggests that our understanding of NO_x is accurate to the 20% level and HO_x chemistry is accurate to the 30% level in the lower stratosphere or better for the POLARIS regime. The behavior of the NO_x and HO_x comparisons to data using steady state versus trajectory chemistry and with updated rate coefficients is discussed in terms of known chemical mechanisms and lifetimes.

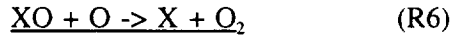
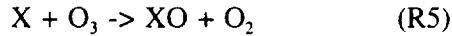
Introduction

Ozone abundances outside the tropical latitudes show a distinct seasonal cycle. In the northern high latitude stratosphere, column ozone abundances decrease from a maximum in late spring to a minimum in early fall [Newman et al., 1997]. To predict trends in ozone and responses of the atmosphere to perturbations such as emissions of a proposed fleet of supersonic transport aircraft [Stolarski et al., 1995], we must understand the processes driving the high latitude seasonal cycle in ozone concentrations.

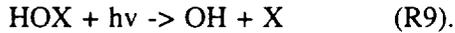
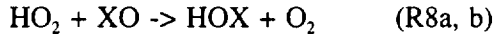
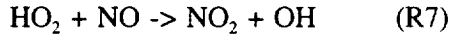
During the summer months, transport of high ozone mixing ratios from low latitudes and high altitudes to the high latitude lower stratosphere is small [Wu, 1987]. Ozone production by photolysis of O_2 is also small relative to tropical latitudes [Johnston, 1975]. With summertime stratospheric temperatures being well above PSC thresholds [Rosenlof, 1996], ozone loss due to chlorine activation on polar stratospheric clouds is unlikely.

The seasonal loss in the northern high latitudes between late spring and fall is generally attributed to in situ photochemical reactions [Perliski, 1989]. The main chemical loss cycles are due to NO_x (NO and NO_2), HO_x (OH and HO_2) with minor contributions from the chlorine and bromine catalytic cycles (in conditions where aerosol is not enhanced by recent volcanic activity). Catalytic loss cycles begin with reactions of NO, OH and halogen atoms with ozone, followed by the loss of an additional odd oxygen (O_3 and O) and reformation of NO, OH, Cl, or Br:

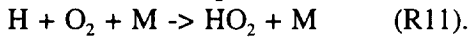
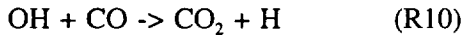




where X = Cl or Br. The HO_x cycle is coupled to NO_x and halogens by the following reactions:



HO_x partitioning also depends on CO



In situ photochemical loss in summertime is primarily due to the NO_x catalytic cycle [Perliski, 1989].

Figure 1 shows the interrelationship of the NO_x species, NO_y reservoirs, and reaction pathways

between them. During the spring and summer, increased solar illumination prevents the formation of N₂O₅ from NO₂ + NO₃ by rapidly photolyzing NO₃, resulting in higher abundances of NO and NO₂.

Figure 1 also shows that species from the other catalytic cycles such as OH and ClO are interrelated with the NO_x cycle. Understanding the reactions and pathways of the NO_x cycle is important not only for assessing ozone loss due to NO_x but also the influence of NO_x on the HO_x and ClO_x catalytic loss cycles.

The POLARIS campaign provides the first ER-2 opportunity to test the photochemistry associated with high latitude ozone loss between spring and fall. At high latitudes in the summer, airmasses experience continuous or near continuous sunlight. Under these conditions, radical species with short lifetimes such as NO_x, HO_x and ClO_x are often assumed to be in steady state. Steady state model calculations have been used in previous ER-2 campaigns to model the diurnal variation of radical species [Salawitch et al., 1994a, b] during the 1993 NASA Stratospheric Photochemistry, Aerosols, and Dynamics Expedition (SPADE) and in the investigation of NO_y partitioning [Gao et al., 1997] during 1994 NASA Airborne Southern Hemisphere Ozone Experiment/Measurements for Assessing the Effects of Stratospheric Aircraft (ASHOE/MAESA). However, the data in some cases is

not accurately described by steady state conditions. Kawa et al. [1993] found that for one high-latitude case, a photochemical model that accounts for latitude and temperature changes 10 days prior to sampling was needed to provide better agreement with observations. In this paper we show how the Goddard trajectory chemistry model can be used to identify POLARIS special cases, put them on a consistent basis with the steady state cases, and in doing so help to separate out systematic biases linked to model chemical mechanisms or rates. Our findings show that use of the trajectory chemistry model reduces the variability of calculated NO_x relative to the steady state model. As a result of the interrelationship between NO_x and HO_x , HO_x variability is reduced also. Trajectory chemistry model results of NO_x are found to be systematically low with respect to the observations using rates from the JPL-97 compendium, consistent with the deficit seen in Gao et al. [1999]. Because the NO_x and HO_x cycles are linked, the NO_x bias must be accounted for before systematic offsets in the HO_x model results can be assessed. Use of the new rate constants of Brown et al. [1999a, b] improves modeled NO_x with observations but agreement of OH and HO_2 individually with observations worsens slightly.

Model Description

The chemistry on trajectory model consists of two parts, a trajectory module [Schoeberl et al., 1993] and a chemistry module [Kawa, et al., 1997]. Using the Goddard assimilated meteorological fields [Algorithm and Theoretical Basis Documents of the Data Assimilation Office, 1997], air parcels intersecting the ER-2 flight path every 432 seconds (~86 km) are advected backwards 10 days. Latitude, longitude, temperature, pressure and solar zenith angle are calculated at 15 minute time steps along the isentropic back trajectory.

The chemistry portion of the model includes 30 species and 120 reactions with reaction rates from the JPL-97-4 compendium [DeMore et al., 1997]. The chemical mechanism is designed for stratospheric conditions. Constituent mixing ratios of long-lived species NO_y , H_2O , CH_4 , O_3 and CO

are initialized from ER-2 measurements [Gao et al., 1997; Hintsä et al., 1998; Webster et al., 1994; Proffitt et al., 1989]. Cl_y and Br_y were estimated from measured N_2O and CFC_3 and the correlations of Woodbridge et al. [1995] and Wamsley et al. [1998]. Initial Cl_y partitioning is set by measured HCl with the balance in $ClONO_2$. Initial ClO concentrations are set to zero. Initial NO_y partitioning is set by measured NO_x , $ClONO_2$ from Cl_y , small fractions in N_2O_5 (0.5% of the NO_y - $ClONO_2$ - NO_x) and HO_2NO_2 (3% of NO_y - $ClONO_2$ - NO_x - $0.1*Br_y$ - N_2O_5) and the remainder in HNO_3 . Initial CH_3OOH is from the Goddard 3D CTM interpolated to the trajectory starting point's latitude and longitude coordinates and H_2O_2 is determined from a fit to measured O_3 . Other species are initially zero or partitioned in instantaneous steady state.

Heterogeneous chemistry parameters are established assuming measured particles are composed of a ternary solution of sulfate, nitrate and water [Kawa et al., 1997]. The parameters are used primarily for the N_2O_5 and $BrONO_2$ hydrolysis reactions whose reaction sticking coefficients are 0.1 and 0.4, respectively, for this analysis. For POLARIS conditions the HNO_3 content of the particles is negligible. H_2SO_4 mixing ratio is obtained from the Focused Cavity Aerosol Spectrometer FCAS [Jonsson et al., 1995] volume by assuming vapor pressure equilibrium [Carslaw et al., 1995]. HNO_3 varies with the chemistry along the back trajectory while H_2SO_4 , measured aerosol number, and H_2O mixing ratios are assumed to be conserved along the back trajectory. Temperature variations along the trajectory produce composition changes leading to a change in the total particle volume. Reactive surface area is calculated from measured particle number and calculated particle volume.

Photolysis rates are obtained from a table look-up based on albedo, overhead ozone, solar zenith angle, pressure and temperature. The tabulated calculations are from the radiative transfer model of Anderson and Lloyd [1990] and Anderson et al. [1995]. Albedo is determined along the back trajectory by interpolating total ozone mapping spectrometer (TOMS) reflectivities to the trajectory's latitude /longitude coordinates. Overhead ozone is determined by scaling climatological

profiles and TOMS data along the trajectories to match overhead ozone from the Composition and Photodissociative Flux Measurement (CPFM) instrument [McElroy, 1995] at the flight track.

The model can be also run fixed in latitude and longitude at the point where the trajectory intersects the flight path. Models run at a fixed point are initialized in the same manner using flight data and the diurnal chemistry proceeds at that point for 20 days. Running the model in this mode is considered to approach steady state as constituents change less than 5% over the last ten days of the model run. We designate the different modes as trajectory chemistry and point chemistry in the discussion of results.

Comparison with PSS model

The photochemical stationary state (PSS) model used in previous ER-2 aircraft campaigns and in POLARIS assumes that each species reaches a balance between production and loss over 24 hours for the temperature, pressure and latitude of a selected point along the flight track integrated over a diurnal cycle [Salawitch, 1994a]. Measured NO_y , O_3 , H_2O , and CH_4 are used to initialize the model, and Cl_y and Br_y are inferred from relationships with CFC and brominated source gases [Woodbridge et al., 1995; Schauffler et al., 1993]. There are 35 reactive species and 200 chemical reactions with rate constants and cross sections based on the JPL-97 compendium. Photolysis rates are calculated using a radiative transfer model that accounts for Rayleigh and aerosol scattering [Prather, 1981; Salawitch et al., 1994a]. Total column ozone and ultraviolet albedo are specified from observations of TOMS or CPFM measurements when available.

Figure 2a is a timeseries plot of NO , NO_2 and NO_x/NO_y observations and model results using JPL-97 rates from the point chemistry model and PSS for the POLARIS flight on July 7, 1997. Steady state conditions were dominant since solar zenith angles were between 55° and 70° and back trajectories show air parcels experience continual sunlight, indicative of high solar exposure and short

NO_x lifetimes (< 1-2 days). The timeseries of NO , NO_2 and NO_x/NO_y shows that the trajectory chemistry model run in the point chemistry mode agrees well with the PSS model results. Point chemistry model results of NO_x agree within 5% of the PSS results. The 5% underestimate of NO_x in the point chemistry model is due to the underestimate of NO_2 . These small differences are traceable to small differences in the albedo and photolysis rates but agreement between both models shows that both models calculate a similar photochemical steady state over a wide latitude range (5-90°N).

Figure 2b is a timeseries plot of OH , HO_2 and OH/HO_2 observations and model results similar to figure 2 for July 7, 1997. The first two panels show that HO_x in the point chemistry model agrees with the PSS model results to within 15%. Although not shown here, this HO_x point chemistry agreement with PSS mode results is consistent for all the POLARIS. HO_x overall, however, is underestimated relative to the observations as seen in the third panel. It is important to recognize that because of the interrelationship between NO_x and HO_x cycles, the bias seen in NO_x influences HO_x and is addressed later.

We extend the analysis between point chemistry and PSS to include flights over the entire mission. Figure 3a shows the scatter plot comparison of modeled NO_x/NO_y using JPL-97 rates from the point chemistry model and PSS. The flights of 970630 and 970710 were not included since they had very few trajectory points above 90 hPa to analyze (< 5). The NO_x/NO_y ratio in the point chemistry model compares to within 3% of the PSS model with a slope and correlation coefficient near 1.0. The point chemistry model can now be used as a reference to steady state to begin examining cases where point chemistry/steady state does not accurately describe observations during POLARIS by comparing results with the trajectory model results.

Figure 3b compares modeled NO_x/NO_y using trajectory chemistry to point chemistry. In general, trajectory chemistry model results agree with or lie above the 1:1 line. However, portions of the flights of April 24 (blue diamonds), April 26 (green triangles), September 8 (green pluses) and

September 21, 1997 (yellow triangles) lie more than 20% off of the 1:1 line. These flights represent cases where point chemistry does not accurately describe the NO_x observations.

NO_x Example flight

The flight of April 26, 1997 during the spring deployment presents an interesting case study for use of trajectory chemistry. The ER-2 flew out of Fairbanks (65°N) to the pole and back with a profile at the pole. Solar zenith angles during the flight were between 55 and 75 degrees and the aircraft sampled the edge of the persistent winter vortex as seen in reduced amounts of CH_4 , N_2O and CO [Webster et al., 1994]. Figure 4 shows the NO , NO_2 and NO_x/NO_y timeseries for the trajectory and point chemistry model results using JPL-97 rates and observations. The latitudes sampled during the flight are shown on the top axis. At first glance, it appears that the observations are in steady state as all three panels show that the point chemistry model is in reasonable agreement with the observations between 64000 and 80000 UT seconds. The trajectory chemistry model does not agree well with the observations, underestimating NO_x . Figure 5 shows 10-day back trajectories of the parcels intersecting the flights path's on the outbound leg of the flight to the pole. Air parcels experienced a strong southerly advection resulting in a large latitudinal excursion over the last few days prior to ER-2 sampling. In such a situation, it is quite likely that the parcels are not in photochemical steady state.

Figure 6 shows the solar zenith angle, NO_x , and HNO_3 histories in the point and trajectory chemistry models for the ten days prior to sampling of parcel 26, marked with an arrow in Figure 4 as P26. In the trajectory model, the air parcel spends time in darkness ($\text{SZA} > 95$) while in the point chemistry model it does not experience darkness at all. The trajectory chemistry model accounts for latitude variations along the back trajectory while the point chemistry model holds the point fixed with no latitudinal variation. The longer time in darkness along the back trajectory results in less photolysis

of HNO_3 , more formation of N_2O_5 , and consequently less NO_x .

For the flight of April 26, 1997, the steady state/point chemistry model agrees well with measured NO_x but for the wrong reason. The difference between the trajectory chemistry model results with observations is a better indicator of the systematic difference between model and actual photochemistry than the point chemistry model, even though the point chemistry model is in closer agreement. Air parcels experienced changes in the solar exposure on time scales much shorter than the time scale for the photochemistry to relax to steady state. Previous steady state modeling results by Gao et al. [1997, 1999] have shown the PSS model to underpredict NO_x/NO_y by 20-30% similar to the comparison with the trajectory chemistry in Figure 4. Comparison of NO_x/NO_y from the chemistry model with all of the POLARIS observations (below) shows that NO_x/NO_y is consistently underestimated by a similar amount.

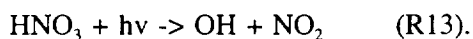
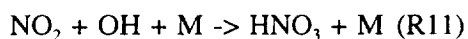
Variability studies

The trajectory chemistry model complements and improves use of the steady state assumption in modeling aircraft data by identifying flights where trajectories influence photochemistry. In these flights, the steady state assumption may not be adequate in modeling those regions. In figure 7, we plot the comparison of the trajectory and point chemistry model results using JPL-97 rates versus all mission observations for NO_x/NO_y . The solid black line represents the one-to-one line and the solid red line denotes a linear least squares fit to the data. The trajectory and point chemistry model results display similar 20-30% deficiency in NO_x relative to the observations indicating that there is a systematic bias associated with the model photochemistry. A closer look at the plots shows that the variability of the trajectory chemistry NO_x/NO_y results about the fit line is less than the variability of the point chemistry model results by ~30% as seen in the differences in the standard deviations about the fit line (0.019 vs 0.013). Since NO_x has a photochemical lifetime of ~ 1 week, it is still adjusting

to changes in photolysis caused by changing latitude. This source of variance in the model-data comparisons is removed using the trajectory chemistry. The analysis shows that, while POLARIS NO_x/NO_y data as a whole may be reasonably well-characterized by steady state, individual cases can vary by 25% or more. By reducing the variability, we are able to better diagnose systematic chemical relationships and assess our understanding of the photochemical processes associated with ozone loss.

Model calculations with new rates

We have seen that trajectory chemistry reduces the NO_x variability but exhibits a systematic bias in the photochemistry. During POLARIS, the increasing solar illumination and warmer temperatures prevent N_2O_5 formation and N_2O_5 hydrolysis from controlling the NO_x/NO_y partitioning [Farman et al., 1985]. Under these conditions, the NO_x/NO_y ratio is controlled primarily by the following reactions:



Recently, Brown et al. [1999a, b] reported rates for R11 that are 10-20% slower than recommended in JPL-97 and rates for R12 that are faster by 40-100% for stratospheric temperatures and pressures. Figure 8 shows the result of incorporating these rates into the trajectory chemistry model for the April 26, 1997 flight. Both NO and NO_2 are increased by approximately 15-25% and are in better agreement than the model using JPL-97 rates for reactions R11-R13 above. Figure 9 plots the comparison of modeled NO_x/NO_y using Brown et al. and observed NO_x/NO_y for the entire mission. The solid black line through the data is the least squares fit. Comparing Figure 9 and the top panel of Figure 7, inclusion of Brown et al. [1999a, b] increases NO_x by 25% and reduces the bias between

modeled NO_x/NO_y and observations by $\sim 70\%$. More NO_x is available as a result of slower loss of NO_2 from reaction R11 and faster production from R12. The agreement of modeled NO_x/NO_y in figure 9 is similar to the improved agreement seen in Gao et al. [1999].

Inclusion of the updated rate constants improves the agreement with observations but a 5-10% bias still exists. Instrumental uncertainties for NO , NO_2 and NO_y [Gao et al., 1997] collectively are on the order of $\pm 40\%$ and so the bias is within experimental error. Other sources of error which may contribute to the bias include input albedo and O_3 column above the ER-2 which are key parameters in establishing the model photochemistry. Albedo influences the partitioning of NO_x between NO and NO_2 through J_{NO_2} (refer to Figure 1) but sensitivity studies show that doubling the albedo results only in a 10% increase in model NO_x . Based on the analysis of TOMS irradiances by Herman and Celarier [1997], the albedo would not be expected to be uncertain by a factor of two. CPFM measurements of overhead ozone have an uncertainty of $\pm 3\%$ [McElroy, 1995] and trajectory model sensitivity studies for POLARIS conditions show a 3% increase/decrease in the overhead column results in a 3% decrease/increase in NO_x abundance. An evaluation of the NO_x production and loss sensitivity to changes in chemical concentration, rate coefficients and radiative conditions sensitivities during POLARIS by Perkins et al. [1999] demonstrated that changing the overhead column by 10% or decreasing the $\text{OH} + \text{NO}_2$ rate constant another 10% would be necessary to reduce the NO_x deficiency. It is pointed out, however, that changes to NO_x and NO_y concentration measurements or photolysis rates may also contribute, thus making it difficult to separate out a single source.

Effects on HO_x

The relationship between the NO_x catalytic cycle and the HO_x species implies that changes in NO_x with the use of the new rates constants should lead to changes in the HO_x . The HO_x production and loss processes are best represented by OH since the majority of the HO_x production and loss

processes involve the OH radical. HO_x production through OH formation is primarily characterized by HNO₃ photolysis and reaction of H₂O with O(¹D) followed by smaller contributions from HNO₄ and CH₂O photolysis at lower solar zenith angles [Hanisco et al., 1999] and contributions from HOBr photolysis at higher solar zenith angles [Wennberg et al., 1999]. The reactions of OH with NO₂, OH with HNO₃ and reaction of HO₂ with NO₂ represent the primary HO_x loss processes [Wennberg et al., 1990, Hanisco et al., 1999].

Use of the Brown et al. rates will affect HO_x directly by the decrease in the $k_{\text{OH}+\text{NO}_2}$ and increase in the $k_{\text{OH}+\text{HNO}_3}$ reaction rates. The reaction of OH + NO₂ is roughly two times as significant as OH + HNO₃ in the loss of HO_x. Since $k_{\text{OH}+\text{HNO}_3}$ increases by twice the amount that $k_{\text{OH}+\text{NO}_2}$ decreases, the rates roughly cancel. HO_x loss rates are affected indirectly by the increased NO₂ and decreased HNO₃ that result from using the new rate constants. The fractional change in NO₂ is large and tends to dominate over the small fractional decrease in HNO₃ so that the net effect is an increase in the HO_x loss rates. Since the OH + NO₂ reaction makes up about half the total loss rate, a 20% increase in NO₂ using the Brown rate constants results in a 10% decrease in OH relative to JPL-97 rates. HO₂ concentrations respond to the changes in the HO_x loss rates but also to changes in the OH/HO₂ partitioning. Increased HO_x loss rates result in lower HO₂ because there is less OH to convert to HO₂ and increased NO_x results in lower HO₂ because HO₂ is converted into OH more quickly.

The effects of trajectory chemistry and the use of the updated rate constants of Brown et al. [1999a, b] on OH, HO₂ and OH/HO₂ can be seen in the statistical results for three model runs presented in Table 1. With the recommended JPL-97 rates, trajectory chemistry reduces the variability of OH by about 20% from 0.051 to 0.040 in the standard deviation about the fit as a result of the reduction in the variability of HNO₃ and NO₂ (see Figure 7). Using trajectory chemistry with the

Brown rate constants, the modeled OH is in lesser agreement than using the JPL-97 rates (-0.222 vs. -0.300) despite the fact that NO_x/NO_y is in better agreement with the observations (see Figure 9). This suggests that there is still a missing source or overestimation of a sink in the model's HO_x production and loss, consistent with Wennberg et al. [1999] who demonstrated underestimates of HO_x but at higher solar zenith angles. Regardless of solar zenith angle, there is an underestimate of HO_x .

OH and HO_2 interconvert more rapidly than HO_x production and loss processes so that OH and HO_2 are in photochemical steady state [Wennberg, 1990]. Cohen et al. [1994] demonstrated that the OH/ HO_2 ratio is well defined by the steady state equation

$$\frac{[\text{OH}]}{[\text{HO}_2]} = \frac{k7[\text{NO}] + k4[\text{O}_3] + k8a[\text{ClO}] + k8b[\text{BrO}]}{k3[\text{O}_3] + k10[\text{CO}]} \quad (1)$$

where $k3$, $k4$, $k7$, $k8$, $k10$ are the rate constants from reactions R3, R4, R7, R8 and R10. For the high latitude summer stratosphere, Lanzendorf et al. [1999] show that equation 1 simplifies to

$$\frac{[\text{OH}]}{[\text{HO}_2]} = \frac{k7[\text{NO}] + k4[\text{O}_3]}{k3[\text{O}_3]} \quad (2)$$

Using the rates of Brown et al., the difference between the modeled and measured OH/ HO_2 decreases (-0.211 to -0.139). Since the updated rate constants increase NO_x , the OH/ HO_2 ratio increases also since it is governed only by the abundance of NO as ozone remains constant to first order.

The effects of trajectory chemistry and inclusion of the Brown rate constants on HO_2 are more dramatic than those seen with OH. Using the JPL-97 rates, the average value of modeled HO_2 is very close to the observed HO_2 and not very different in going from point chemistry to trajectory chemistry (0.005 vs -0.006). However, trajectory chemistry reduces the modeled HO_2 variability more than it reduces the OH variability (0.61-0.41/0.61 33% vs 0.051-0.040/0.51 22%). Trajectory chemistry has more of an effect since HO_2 abundances are primarily controlled by NO_x through the rapid

repartitioning reaction of $\text{HO}_2 + \text{NO} \rightarrow \text{OH} + \text{NO}_2$. As the NO_x variability improves, the HO_2 variability improves as well. Replacing the JPL-97 rate constants with the updated rate constants of Brown et al. worsens the agreement between modeled and observed HO_2 (-0.006 to -0.185). The change in the modeled HO_2 with the trajectory chemistry using the Brown rate constants is greater than the change in the modeled OH (-0.222 to -0.300 vs -0.006 to -0.185) since the Brown chemistry affects HO_x sources and sources as well as the partitioning between OH and HO_2 .

The sensitivity of HO_x to changes in model parameters is different than the sensitivity of NO_x . While albedo is important in partitioning NO_x into NO and NO_2 as shown by Schwartz et al [1999], sensitivity studies show that tripling the albedo from 0.2 to 0.6 only results in a 15% decrease in the HO_x species. As discussed earlier, uncertainties in the albedo are unlikely to be of this magnitude and should not contribute to the modeled to observed HO_x discrepancy. Sensitivity studies of CPFM measurements of overhead ozone show that a 10-15% increase/decrease in the overhead column results in a 10-15% decrease/increase in HO_x since solar flux is important in the key HO_x production processes involving the formation of $\text{O}(^1\text{D})$ from ozone [Schwartz et al., 1999] for reaction with H_2O and CH_4 and photolysis of HNO_3 , and HNO_4 . It is important to note that due to the coupling between the HO_x and NO_x families, potential errors in HO_x can affect NO_x production and loss as well. NO_x production is primarily characterized by HNO_3 photolysis and reaction with OH and NO_x loss by the reaction of NO_2 with OH and BrONO_2 hydrolysis. Sensitivity studies by Perkins et al. [1999] have shown that a 10% increase/decrease in the OH concentration decreases/increases the production to loss ratio by 5%. Overall, modeled HO_x agreement with observations is within the measurement uncertainties using the Brown rate constants.

Conclusion

The POLARIS mission was designed to study chemical ozone loss processes which are accelerated as a result of increased solar illumination at summer high latitudes. NO_x is primarily responsible for this stratospheric loss from late spring to early fall at high latitudes. Two useful tools for analyzing the radical abundances observed during POLARIS are the steady state and trajectory chemistry models. The trajectory chemistry model, initialized from observations and run in the fixed point mode agrees well with a steady state model, establishing a consistent basis from which we can begin to separate out the effects from trajectories and systematic biases in the photochemistry. An investigation of all mission flights revealed that as a whole POLARIS data could be adequately characterized by steady state but that trajectory history influences radical abundances significantly in several flights. The point chemistry model produces too much NO_x as a result of longer, more consistent sun exposure than the shorter, more variable sun exposures encountered when trajectory history is taken into account. A comparison of the trajectory and point chemistry model results with the observations demonstrates that using the trajectory model reduces the variability in the NO_x model results and is valuable in constraining relationships among the radical species. However, the trajectory chemistry model results consistently show a NO_x deficiency representing a systematic bias in the photochemistry as in other steady state model results. The variability of HO_x (OH and HO_2) is reduced with trajectory chemistry because of the reduced variability in NO_x and HNO_3 but OH is systematically low compared to observations by 20%. The NO_x bias must be accounted for to properly assess the HO_x chemistry in the model.

To address the systematic bias in NO_x , we included the new rate constants of Brown et al. [1999a, b] for $\text{OH} + \text{NO}_2$ and $\text{OH} + \text{HNO}_3$ in the trajectory chemistry model. Use of these rate constants improves the agreement of modeled NO_x with observations to within the uncertainties of the measurements ($\pm 40\%$) but a small bias (5-10%) still exists. The OH/HO_2 ratio agreement with

observations improves with the new rate constants since the ratio is explicitly dependent on NO.

Inclusion of Brown et al. rates increases the model offset of OH and HO₂ individually relative to observations, consistent with the underestimate in HO_x seen by Wennberg et al [1999] and linked to a missing source in the current photochemistry used in models. The offsets of OH, HO₂ and OH/HO₂, however, are as a whole still within the 2-sigma measurement uncertainties of 25, 30, and 14%, respectively.

References

- Anderson, D. E., Jr., and S. A. Lloyd, Polar twilight UV-visible radiation field: Perturbations due to multiple scattering, ozone depletion, stratospheric clouds and surface albedo, *J. Geophys. Res.*, 95, 7429-7434, 1990.
- Anderson, D. E., R. DeMajistre, S. A. Lloyd, and P. K. Swaminathan, Photodissociation in the troposphere and stratosphere: Radiation field models for clouds, aerosols and twilight., *J. Geophys. Res.*, 100, 7135-7145, 1995.
- Brown, S. S., R. K. Talukdar, and A. R. Ravishankara, Rate constants for the reaction $\text{OH} + \text{NO}_2 + \text{M}$ to $\text{HNO}_3 + \text{M}$ under atmospheric conditions, *Chem Phys. Lett.*, 299 (3-4), 277-84, 1999a.
- Brown, S. S., R. K. Talukdar, and A. R. Ravishankara, Reconsideration of the rate constant for the reaction of the hydroxyl radical with nitric acid, *J. Phys. Chem A.*, 103, 3031-3037, 1999b.
- Carslaw, K. S., B. P. Luo, and T. Peter, An analytic expression for the composition of aqueous HNO_3 - H_2SO_4 stratospheric aerosols including gas phase removal of HNO_3 , *Geophys. Res. Lett.*, 22, 1877-1880, 1995.
- Cohen, R. C., et al., Are models of catalytic removal of O_3 by HO_x accurate? Constraints from in situ measurements of the OH to HO_2 ratio?, *Geophys. Res. Lett.*, 21, 2539-2542, 1994.
- DeMore, W. B., S. P. Sander, D. M. Golden, R. F. Hampson, M. J. Kurylo, C. J. Howard, A. R. Ravishankara, C. E. Kolb, and M. J. Molina, Chemical kinetics and photochemical data for use in stratospheric modeling, JPL Publ., 97-4, Jet Propulsion Laboratory, Pasadena, CA, 1997.
- Farman, J. C., R.J. Murgatroyd, A. M. Silnickas, B. A. Thrush, Ozone photochemistry in the Antarctic stratosphere in summer, *Quart. J. R. Met. Soc.*, 111, 1013-1028, 1985.
- Gao, R. S., et al., Partitioning of the reactive nitrogen reservoir in the lower stratosphere of the southern hemisphere: Observations and modeling, *J. Geophys. Res.*, 102, 3935-3949, 1997.

- Gao, R. S., et al., A comparison of observations and model simulations of NO_x/NO_y in the lower stratosphere, *Geophys. Res. Lett.*, submitted, 1998.
- Herman, J. R. and E. A. Celarier, Earth surface reflectivity climatology at 340-380 nm from TOMS data, *J. Geophys. Res.*, 102, 28003-28011, 1997.
- Hints, E. J., et al., Tropospheric to stratospheric transport in the lowermost stratosphere from measurements of H_2O , CO_2 , N_2O , and O_3 , *Geophys. Res. Lett.*, 25, 2655-2658, 1998.
- Kawa, S. R., et al., Interpretation of NO_x/NO_y observations from AASE-II using a model of chemistry along trajectories, *Geophys. Res. Lett.*, 22, 2507-2510, 1993.
- Kawa, S. R., et al., Activation of chlorine in sulfate aerosol as inferred from aircraft observations, *J. Geophys. Res.*, 102, 2949-2955, 1997.
- Hanisco, T. F., et al., Sources, sinks and the distribution of OH in the lower stratosphere, in preparation, 1999.
- Johnston, H. S., Global ozone balance in the natural stratosphere, *Rev. Geophys. Space Phys.*, 13, 637-649, 1975.
- Jonsson, H. H., et al., Performance of a focused cavity aerosol spectrometer for measurements in the stratosphere of particle size in the 0.06-2.0 μm diameter range, *J. Atmos. Oceanic Tech.*, 12, 115-129, 1995.
- Lanzendorf, E. J., et al., Establishing the dependence of HO_2/OH on temperature, halogen loading, ozone, and NO_x based on in situ measurements from the NASA ER-2, submitted to *J. Geophys. Res.*, 1999.
- McElroy, C. T., A spectroradiometer for the measurement of direct and scattered solar irradiance from on-board the NASA ER-2 high-altitude aircraft, *Geophys. Res. Lett.*, 22, 1361-1364, 1995.
- Newman, P. A., J. F. Gleason, R. D. McPeters, and R. S. Stolarski, Anomalously low ozone over the Arctic, *Geophys. Res. Lett.*, 24, 2689-2692, 1997.

- Perkins, K. K., et al., An examination of the NO₂/HNO₃ ratio in the lower stratosphere during periods of continuous sunlight: Insights from in situ measurements, submitted to *J. Geophys. Res.*, 1999.
- Perliski, L. M., S. Solomon and J. London, On the interpretation of the seasonal variation of stratospheric ozone, *Planet. Space Sci.*, 37, 1527-1538, 1989.
- Prather, M. J., Ozone in the upper stratosphere and mesosphere, *J. Geophys. Res.*, 86, 5325-5338, 1981.
- Proffitt, M. H., et al., In situ ozone measurements within the 1987 Antarctic ozone hole from a high-altitude ER-2 aircraft, *J. Geophys. Res.*, 94, 16547-16555, 1989.
- Rosenlof, K. H., Summer hemisphere differences in temperature and transport in the lower stratosphere, *J. Geophys. Res.*, 101, 19129-19136, 1996.
- Salawitch, R. J., et al., The distribution of hydrogen, nitrogen and chlorine radicals in the lower stratosphere: Implications for changes in O₃ due to emission of NO_y from supersonic aircraft, *Geophys. Res. Lett.*, 21, 2547-2550, 1994a.
- Salawitch, R. J., et al., The diurnal variation of hydrogen, nitrogen and chlorine radicals: Implications for the heterogeneous production of HNO₂, *Geophys. Res. Lett.*, 21, 2551-2554, 1994b.
- Schauffler, S. M., L. E. Heidt, W. H. Pollock, T. M. Gilpin, J. F. Vedder, S. Solomon, R. A. Lueb, and E. L. Atlas, Measurements of halogenated organic compounds near the tropical tropopause, *Geophys. Res. Lett.*, 20, 2567-2570, 1993.
- Schoeberl, M. R., S. D. Doiron, L. R. Lait, P. A. Newman, and A. J. Krueger, A simulation of the Cerro Hudson SO₂ cloud, *J. Geophys. Res.*, 98, 2949-2955, 1987.
- Schwartz, W. H., S. A. Lloyd, T. L. Kusterer, D. E. Anderson, C. T. McElroy, and C. Midwinter, A sensitivity study of photolysis rate coefficients during POLARIS, submitted to *J. Geophys. Res.*, 1999.

- Stolarski, R.S., et al., 1995 Scientific Assessment of the Atmospheric Effects of Stratospheric Aircraft, NASA Ref. Pub. 1381, 1995.
- Wamsley, P. R., et al., Distribution of halon-1211 in the upper troposphere and lower stratosphere and the 1994 bromine budget, *J. Geophys. Res.*, 103, 1513-1526, 1998.
- Webster, C. R., R. D. May, C. A. Trimble, R. G. Chave, J. Kendall, Aircraft ER-2 laser infrared absorption spectrometer for in situ stratospheric measurements of HCl, N₂O, CH₄, NO₂ and HNO₃, *Appl. Opt.*, 33, 454-472, 1994.
- Wennberg, P. O., R. M. Stimpfle, E. M. Weinstock, A. E. Dessler, S. A. Lloyd, L. B. Lapson, J. J. Schwab, and J. G. Anderson, Simultaneous in situ measurements of OH, HO₂, O₃, and H₂O: A test of modeled stratospheric HO_x chemistry, *Geophys. Res. Lett.*, 17, 1909-1912, 1990.
- Wennberg, P.O., et al., Twilight observations suggest unknown sources of HO_x, *Geophys. Res. Lett.*, in press, 1999.
- Woodbridge, E. L., et al., Estimates of total organic and inorganic chlorine in the lower stratosphere from in situ and flask measurements during AASE-II, *J. Geophys. Res.*, 100, 3057-3064, 1995.
- Wu, M. F., M.A. Geller, J.G. Olson, and E. M. Larson, A study of global ozone transport and the role of planetary waves using satellite data, *J. Geophys. Res.*, 3081-3097, 1987.

Figure Captions

Figure 1. Schematic of the main reaction pathways for NO_y species in the lower stratosphere.

Figure 2. (a) Timeseries plot of NO , NO_2 and NO_x/NO_y for the flight of July 7, 1997. (b) Timeseries plot of OH , HO_2 , OH/HO_2 for the flight of July 7, 1997. Latitude covered during flight is noted on top y-axis. Solid line denotes observations, dash-dot line represents the model results from the photochemical steady state model of Salawitch (1994a) using JPL-97 rates and the dotted line represents the model results from the Goddard trajectory model run in the fixed point mode using JPL-97 rates.

Figure 3. (a) Scatter plot of GSFC point chemistry NO_x/NO_y model results versus JPL photochemical steady state model results for all mission flights. Data below 90 hPa excluded. Specific flights denoted in legend with the date in year, month day format (YYMMDD). Solid black line represents 1:1 line and solid red line denotes linear least squares fit to the data. (b) Scatter plot of trajectory chemistry versus point chemistry NO_x/NO_y using JPL-97 for all mission flights. Solid black line represents 1:1 line and solid red line denotes linear least squares fit to the data.

Figure 4. Timeseries plot of NO , NO_2 and NO_x/NO_y for the flight of 970426. Latitude covered during flight is noted on top y-axis. Small black dots denote observations, dotted line represents the model results from the Goddard trajectory chemistry model run at a fixed point (point chemistry) using JPL-97 rates and the dash-dot line represents the model results from the Goddard trajectory model using JPL-97 rates. The position in the time series of parcel 26 is denoted by the arrow P26 at 70500 UT sec.

Figure 5. Back trajectory plot for points along the ER-2 flight track on the outbound leg from Fairbanks, AK (parcel 0) to the pole (parcel 30). Arrow heads mark trajectory positions every 24 hours at 00z.

Figure 6. Comparison between the trajectory and point chemistry model history of (a) solar zenith angle, (b) NO_y species and (c) HNO_3 for parcel 26 marked in Figure 4.

Figure 7. Scatter plot of modeled NO_x/NO_y using trajectory chemistry with JPL-97 rates and point chemistry with JPL-97 rates versus measured NO_x/NO_y for the POLARIS mission. The legend of Figure 3 describes the figures for each flight. Solid black line represents the 1:1 line and solid red line represents the linear least squares fit to the data.

Figure 8. Timeseries plot of NO , NO_2 and NO_x/NO_y for the flight of 970426. Latitude covered during flight is noted on top y-axis. Small black dots denote observations, dash-dot line represents the model results from the Goddard trajectory model using JPL-97 rates and the dotted line represents the results from the Goddard trajectory chemistry model with the rates of Brown et al. (1999a, b).

Figure 9. Scatter plot of modeled NO_x/NO_y using trajectory chemistry with Brown et al. rates (1999a, b) versus measured NO_x/NO_y for the POLARIS mission. Solid black line through the entire plot represents the 1:1 line and solid line through the data represents the linear least squares fit to the data.

Table 1. Statistics of modeled OH, HO₂, and OH/HO₂ using point and trajectory chemistry with JPL-97 and Brown 1999 rates versus observed OH, HO₂ and OH/HO₂.

| | Point JPL-97 | Traj JPL-97 | Traj Brown 99 |
|--------------------------|-------------------------|------------------------|--------------------------|
| OH | | | |
| Avg % diff (Mod-obs/obs) | -0.220 | -0.222 | -0.300 |
| Slope | 0.842 | 0.831 | 0.762 |
| Y-int | 0.024 | 0.019 | 0.025 |
| Sdev about fit | 0.051 | 0.040 | 0.040 |
| Sdev about 1:1 | 0.135 | 0.134 | 0.182 |
| HO₂ | | | |
| Avg % diff (Mod-obs/obs) | 0.005 | -0.006 | -0.185 |
| Slope | 0.980 | 0.978 | 0.852 |
| Y-int | 0.097 | 0.063 | 0.087 |
| Sdev about fit | 0.612 | 0.417 | 0.348 |
| Sdev about 1:1 | 0.615 | 0.420 | 0.716 |
| OH/HO₂ | | | |
| Avg % diff (Mod-obs/obs) | -0.213 | -0.211 | -0.139 |
| Slope | 0.703 | 0.679 | 0.824 |
| Y-int | 0.013 | 0.017 | 0.006 |
| Sdev about fit | 0.014 | 0.013 | 0.016 |
| Sdev about 1:1 | 0.046 | 0.046 | 0.032 |

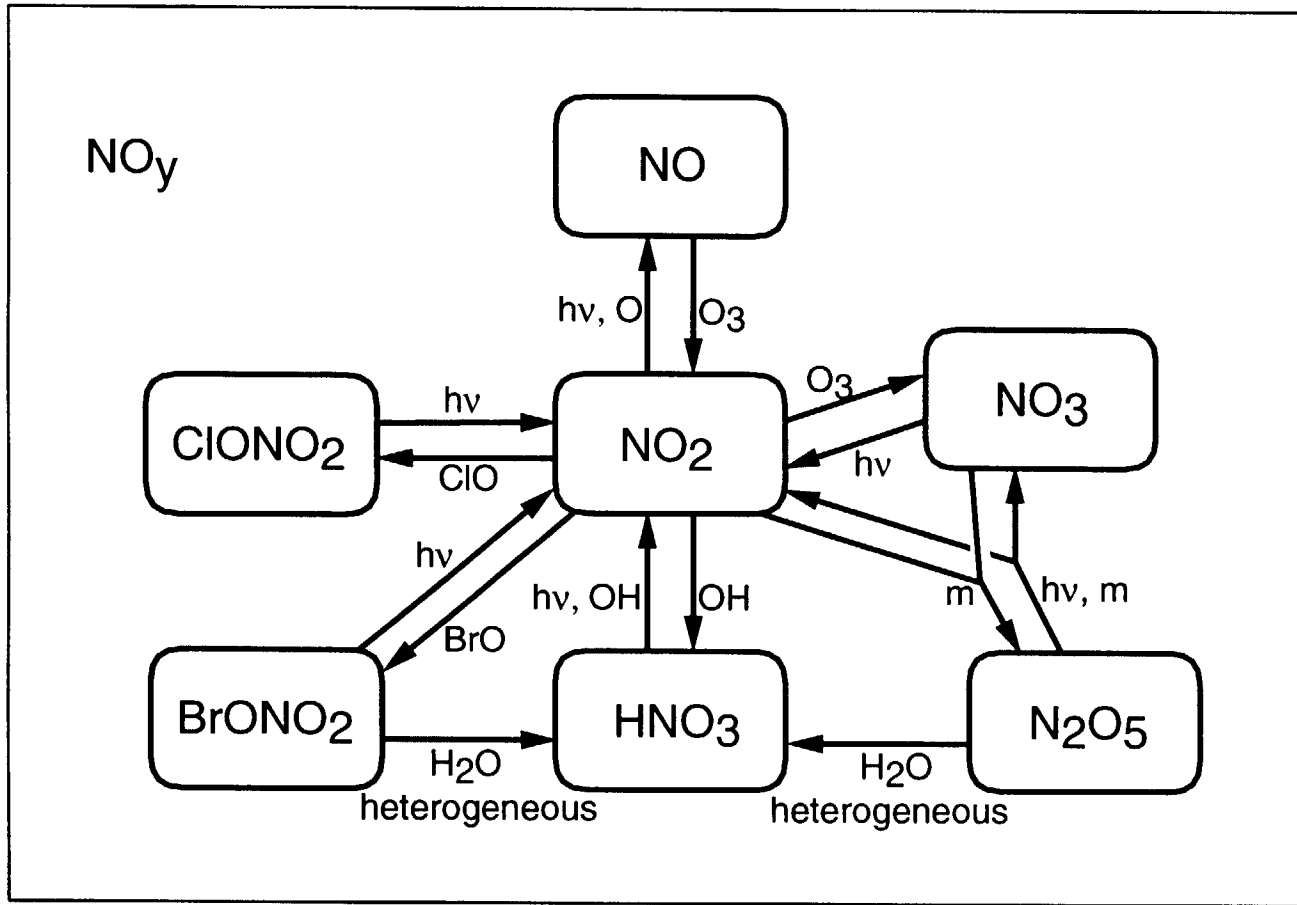


Figure 1

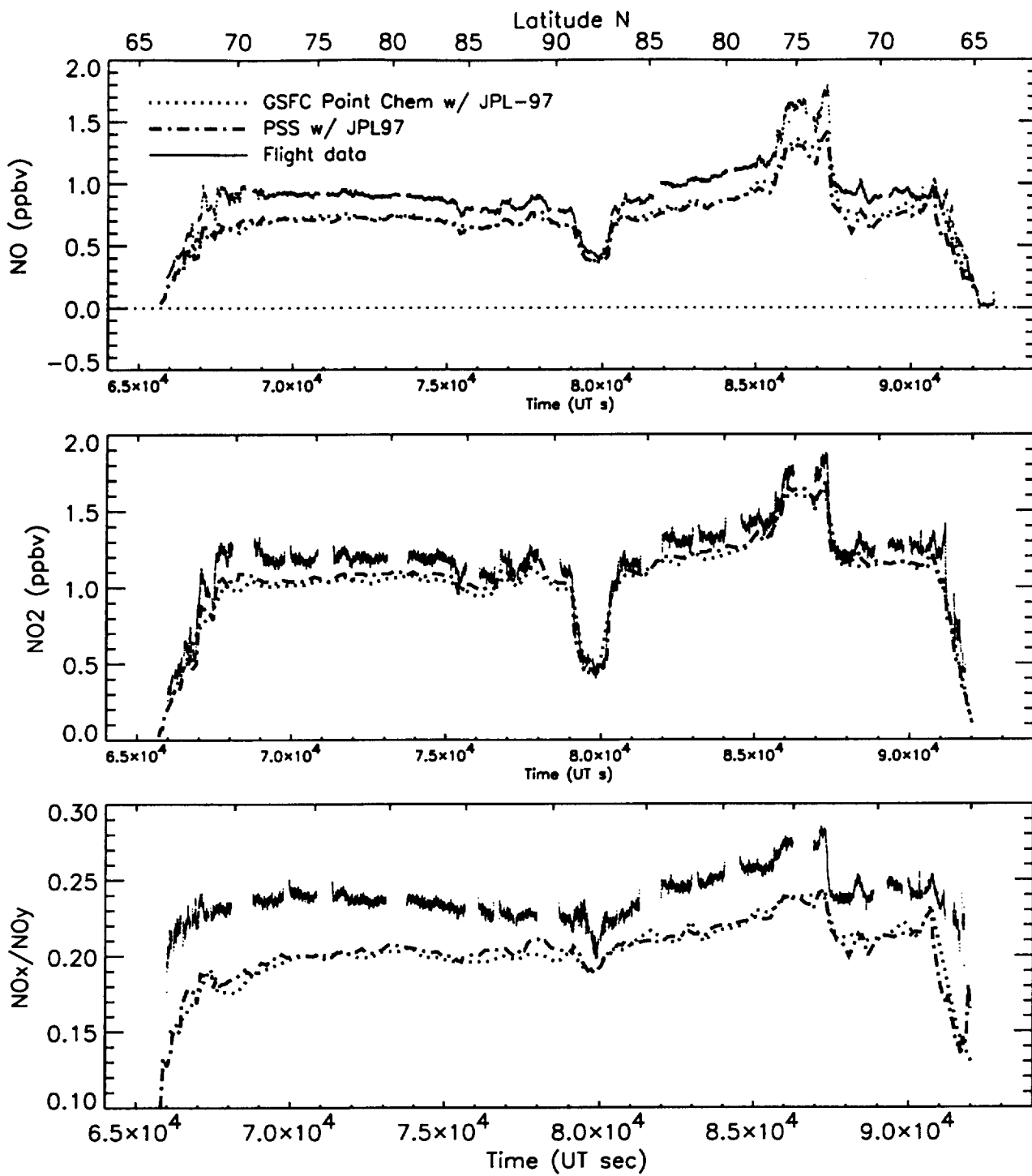


Figure 2a

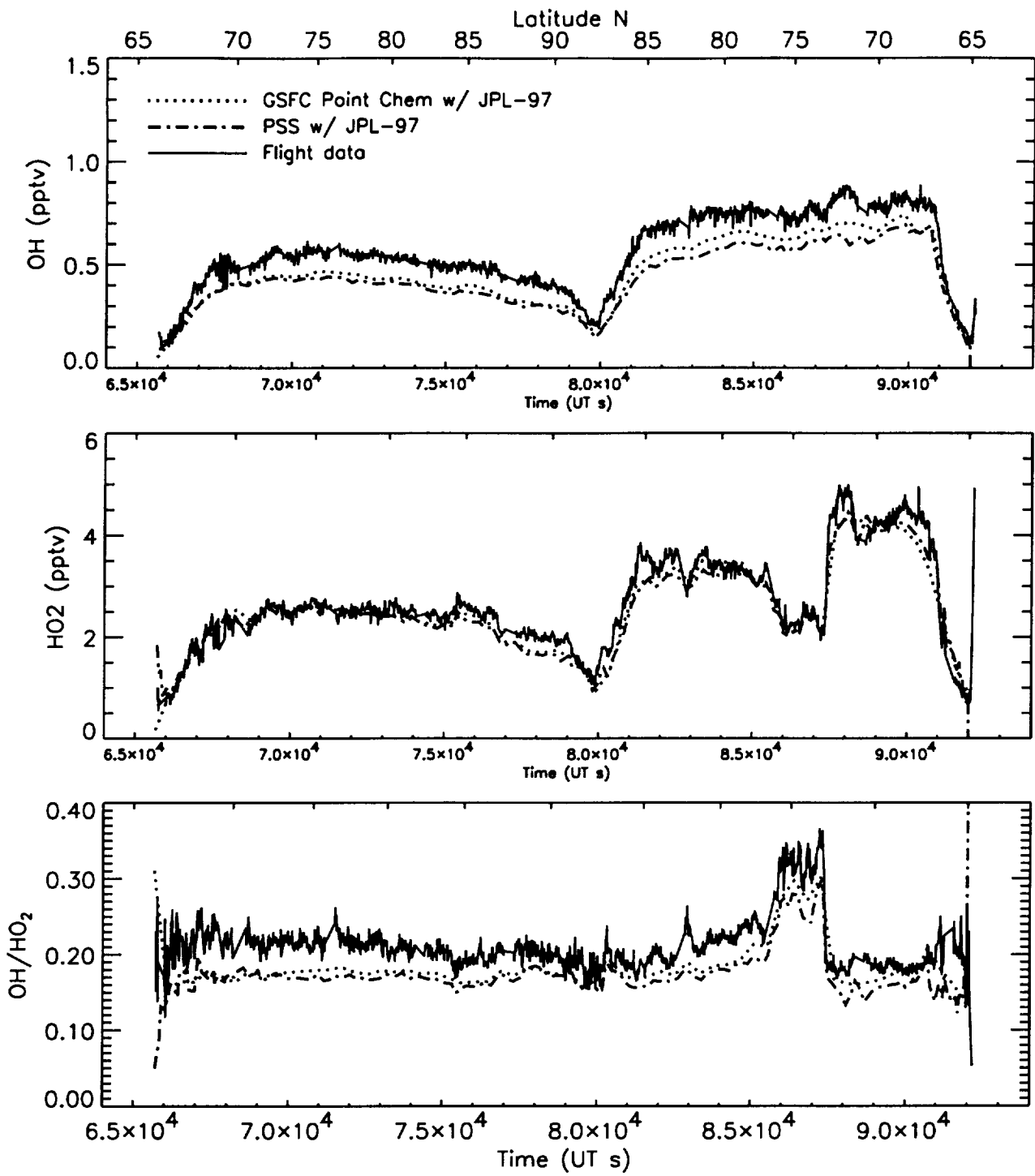


Figure 2b

Point Chem vs. PSS NOx/NOy with JPL-97 rates

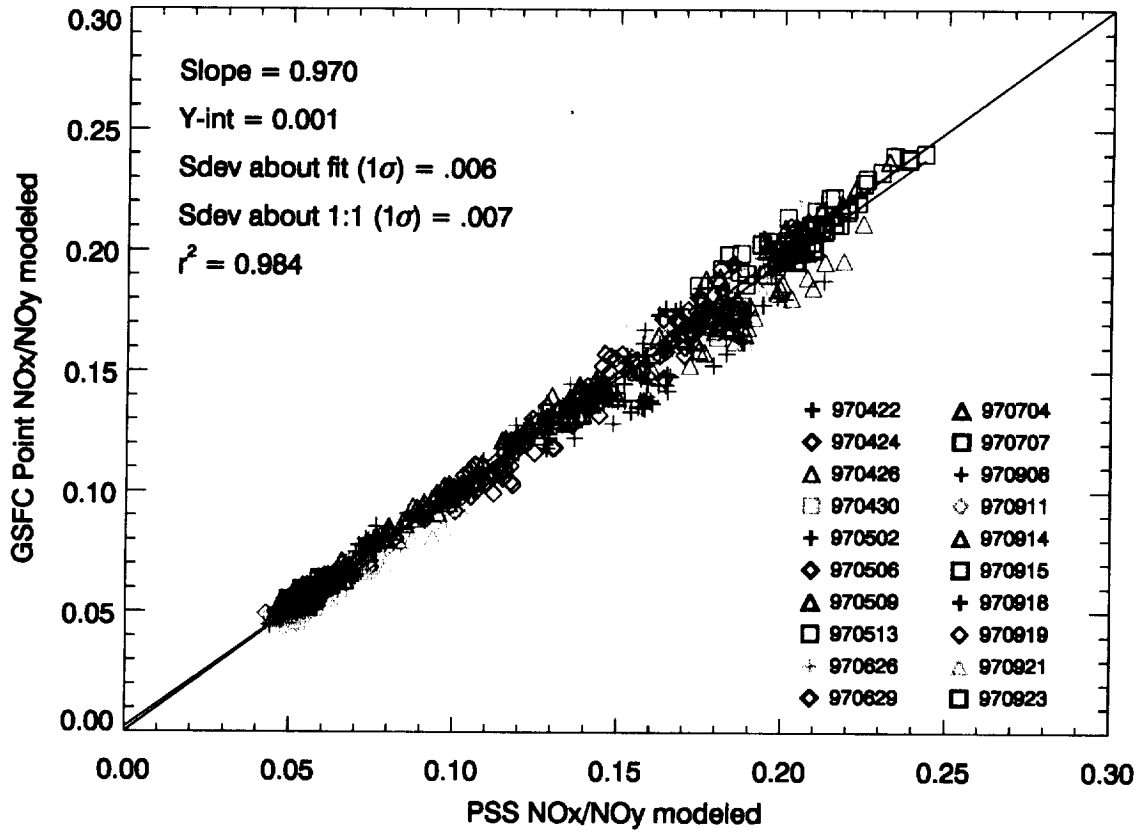


Figure 3a

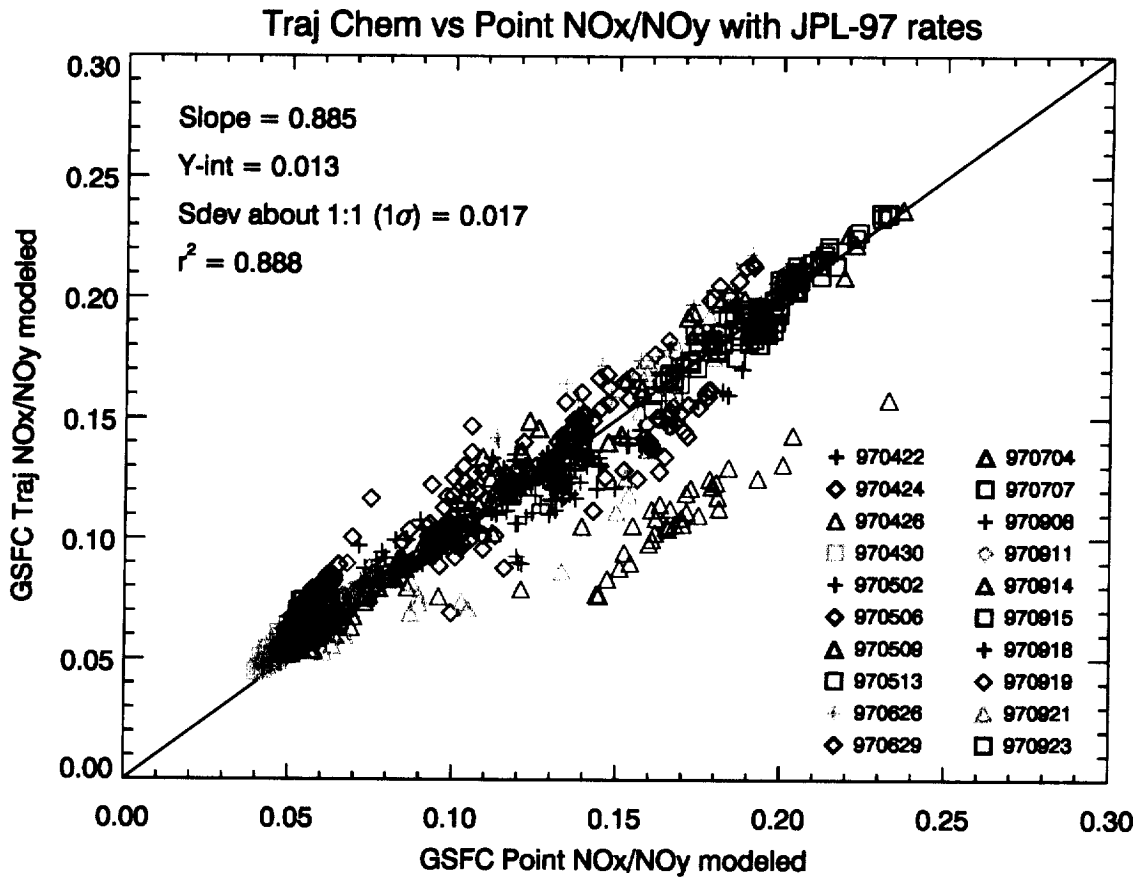


Figure 3b

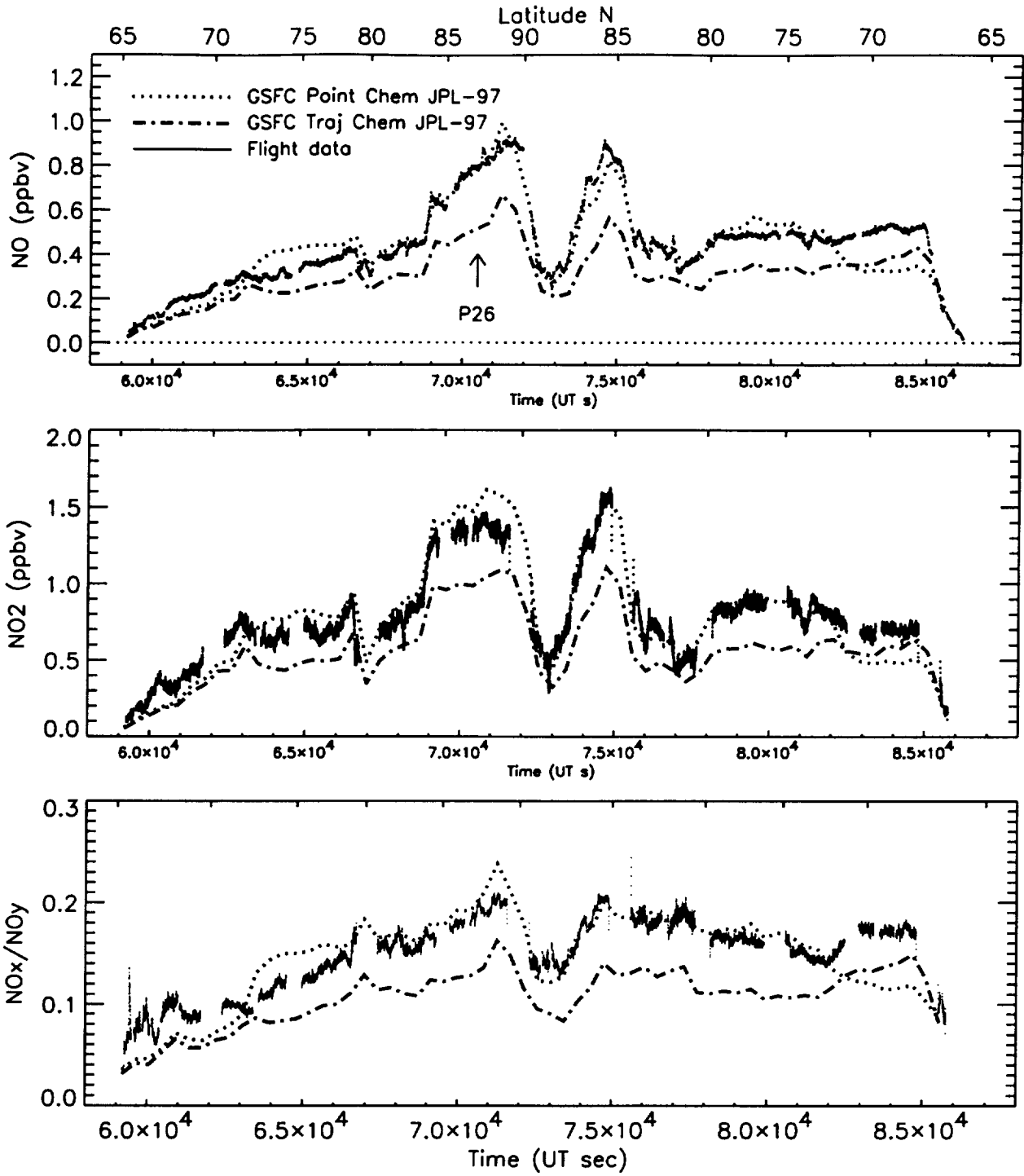
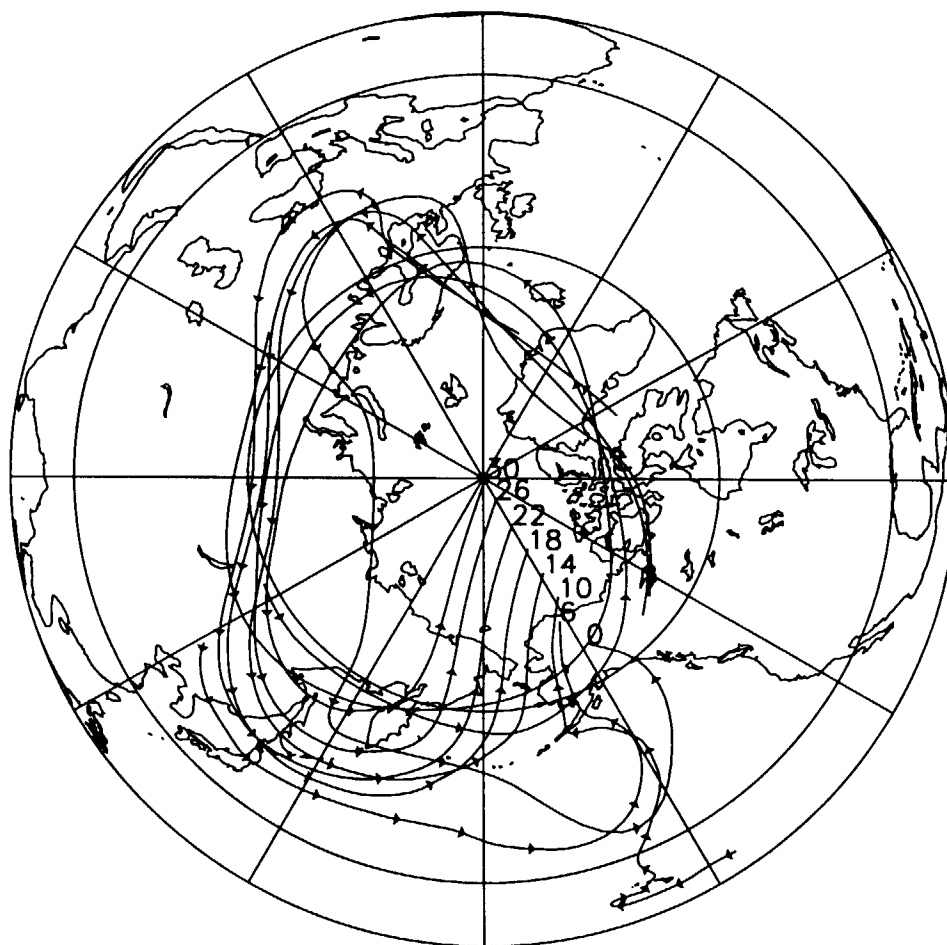


Figure 4

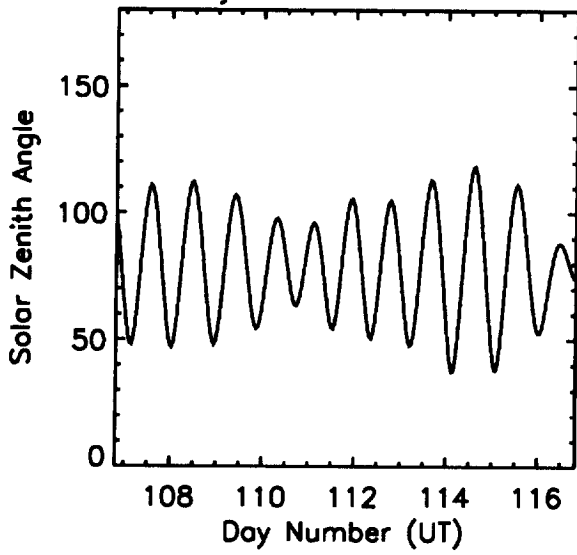
10-Day Back Trajectories for 970426



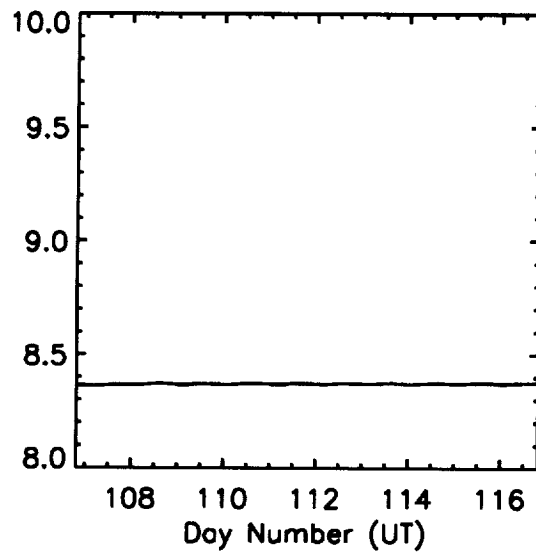
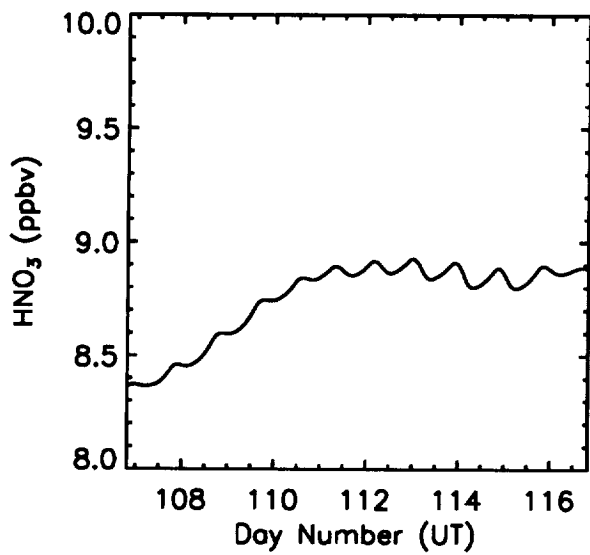
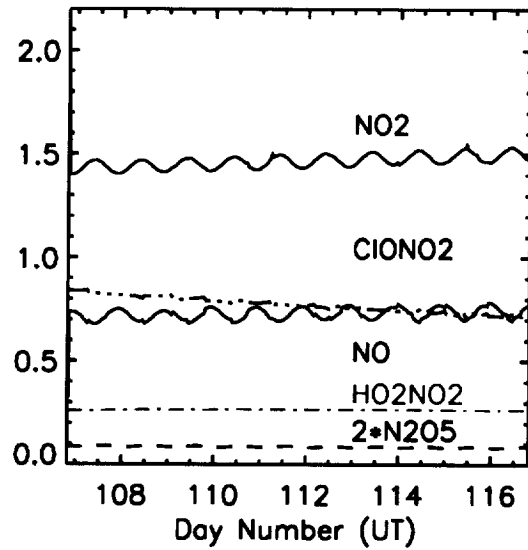
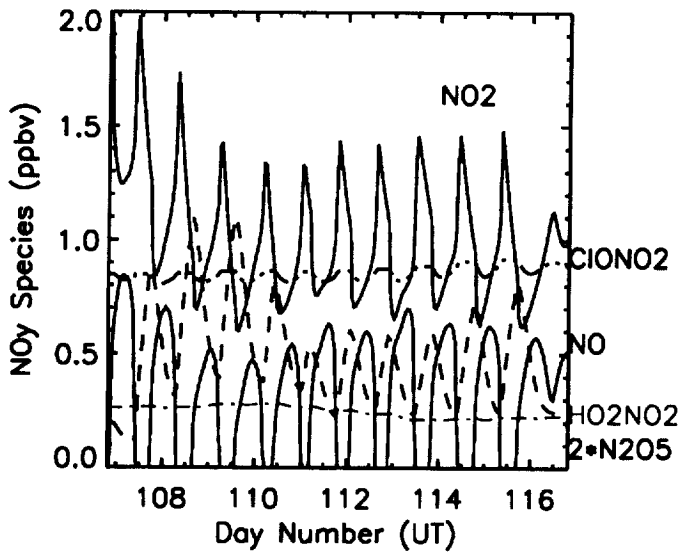
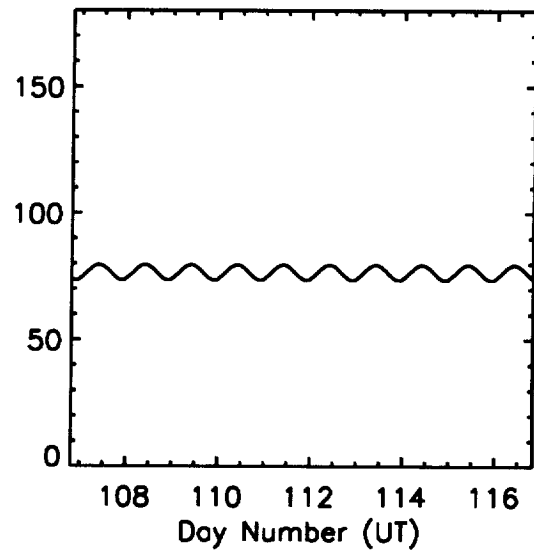
| Parcel | Theta (K) |
|--------|-----------|
| 0 | 349.0 |
| 6 | 493.0 |
| 10 | 502.0 |
| 14 | 502.0 |
| 18 | 507.0 |
| 22 | 504.0 |
| 26 | 500.0 |
| 30 | 481.0 |

Figure 5

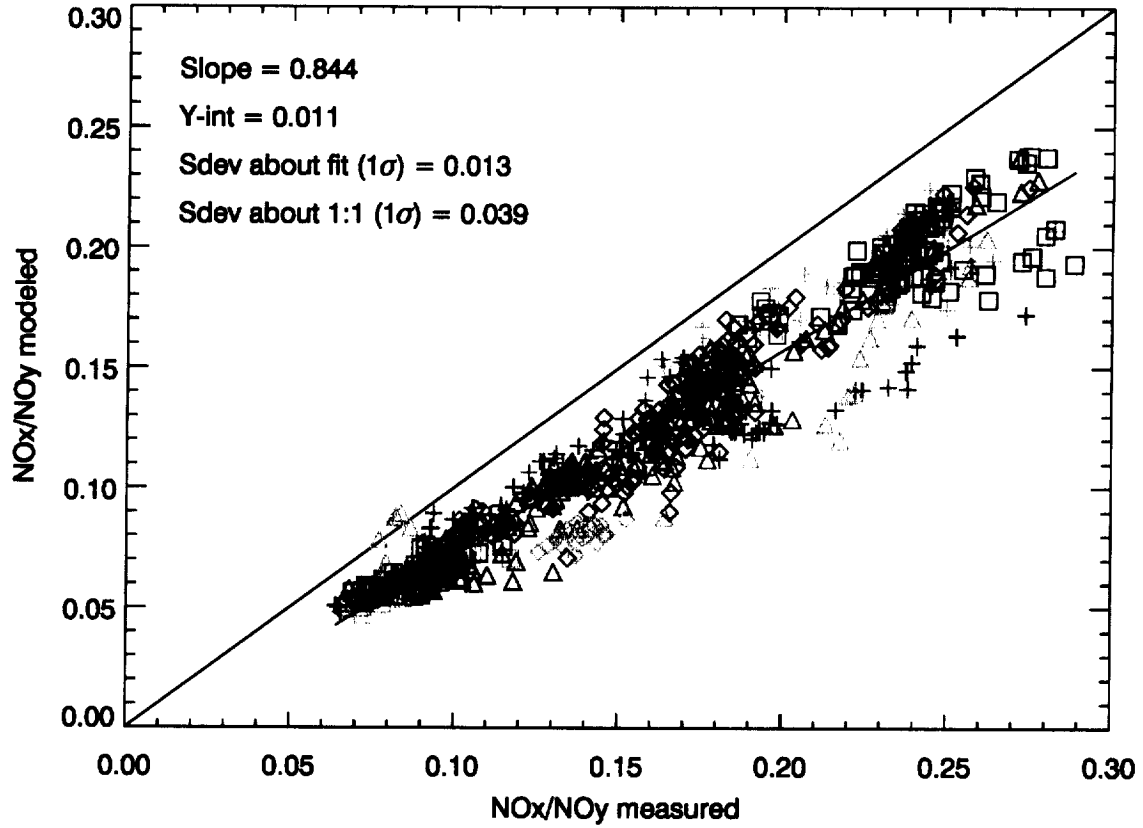
Traj Chem Parcel 26



Point Chem Parcel 26



Traj Chem NO_x/NO_y with JPL-97 rates



Point Chem NO_x/NO_y with JPL-97 rates

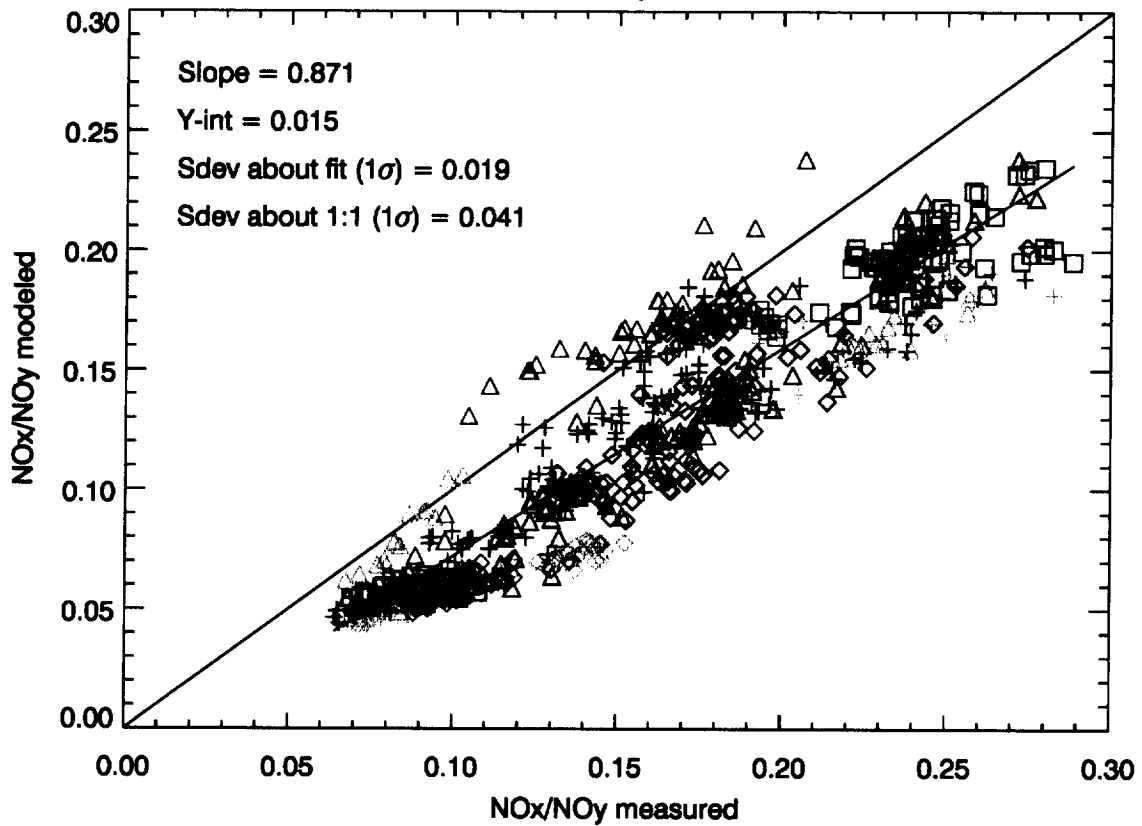


Figure 7

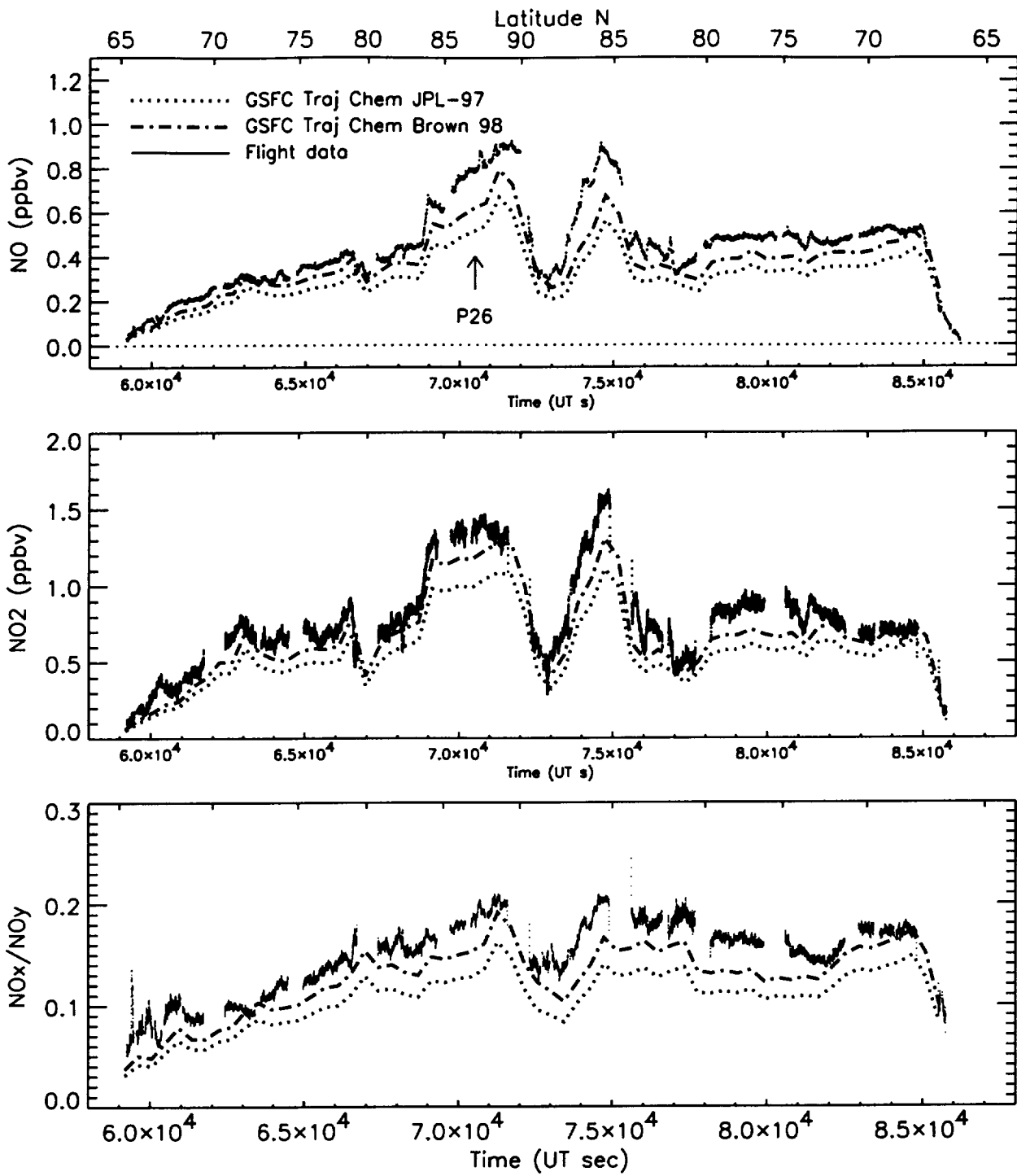


Figure 8

Traj Chem NO_x/NO_y with Brown 98 rates

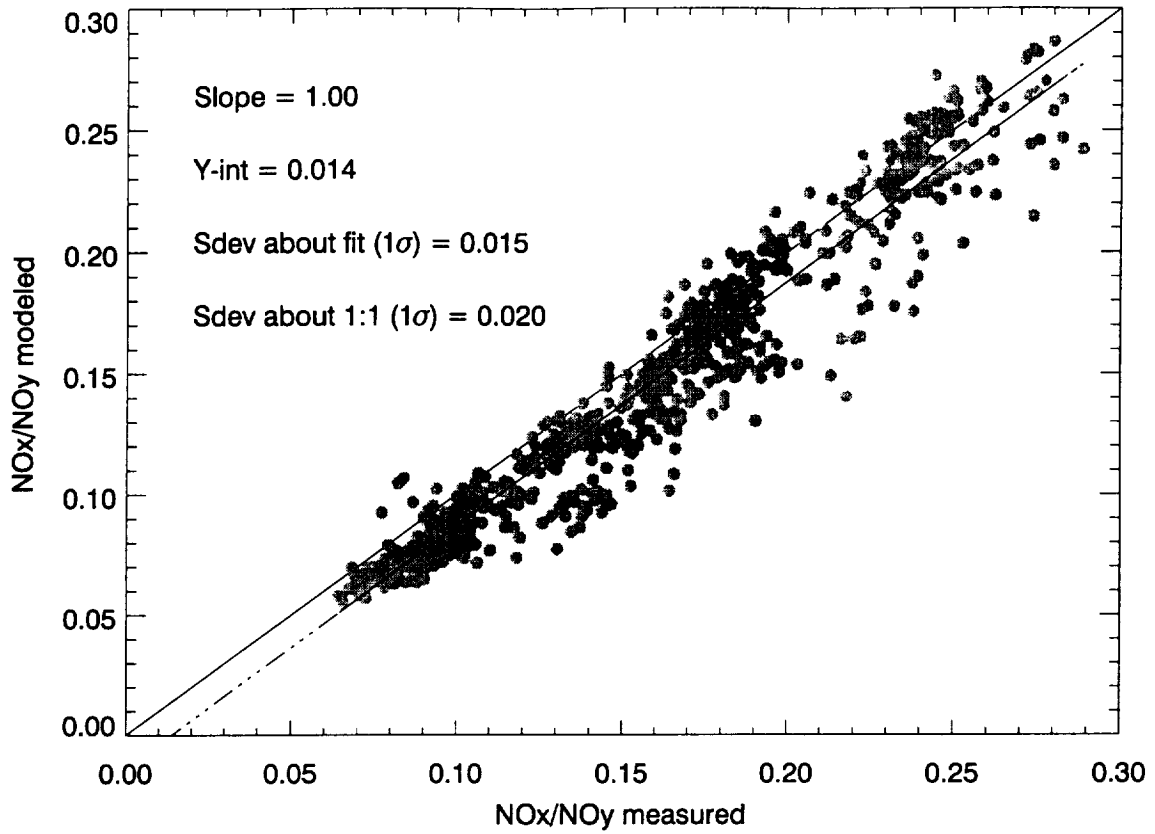


Figure 9